THE TALBOT EFFECT AND THE EVOLUTION OF VORTEX FILAMENTS

Luis VEGA, BCAM-UPV/EHU

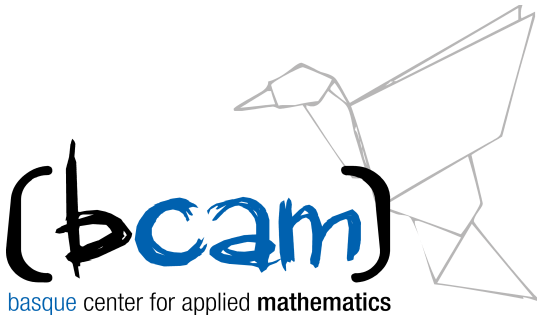

MSRI, October 20, 2015

- Vortex Filaments
- One corner (with V. Banica)
- Regular Polygon (with F. De la Hoz)
- The Talbot Effect
- Turbulence:
  - (Pseudo) randomness
  - Intermittency/multifractality
  - Transfer of energy (cascade)

Q: Has the Talbot effect anything to do with turbulence?

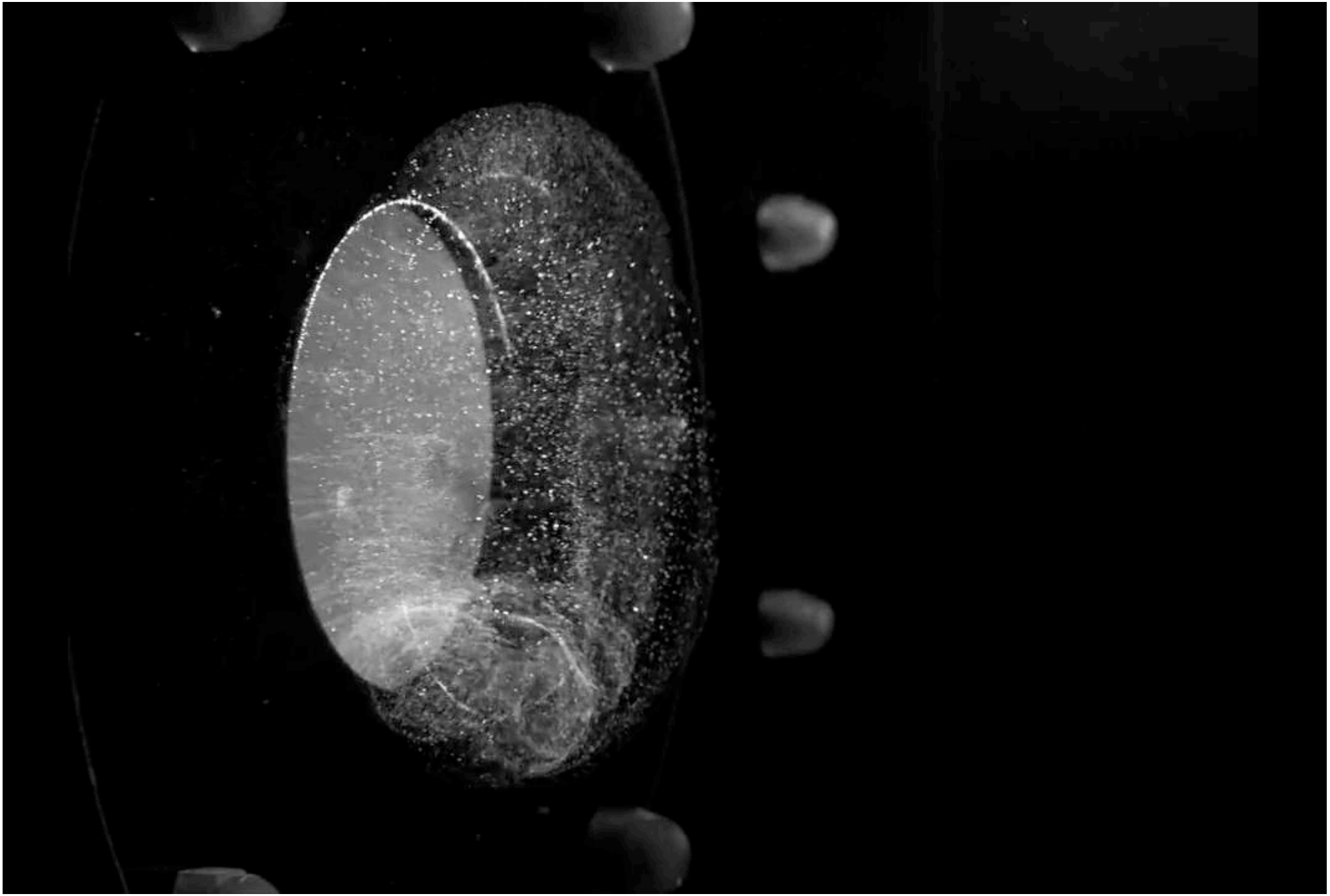

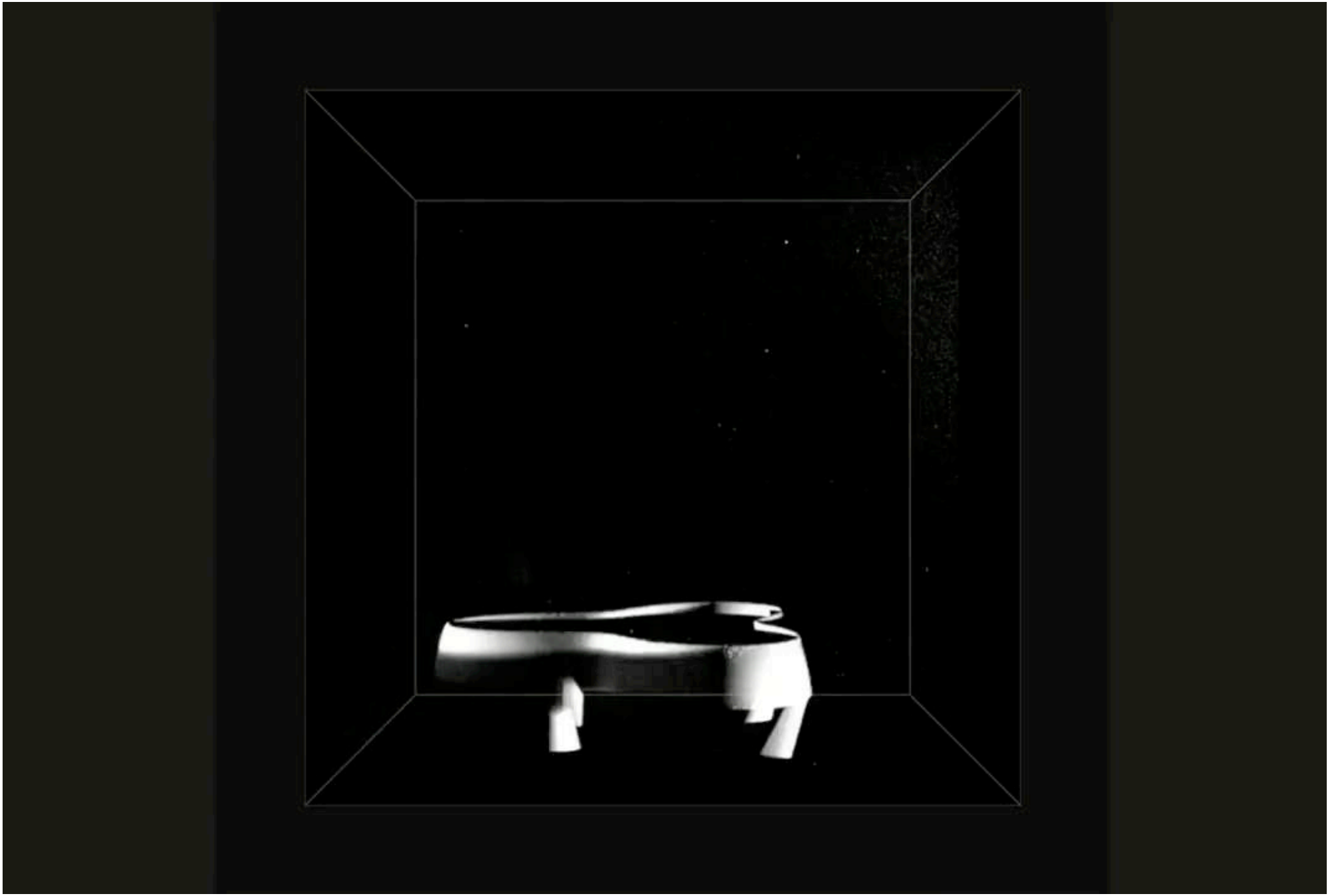

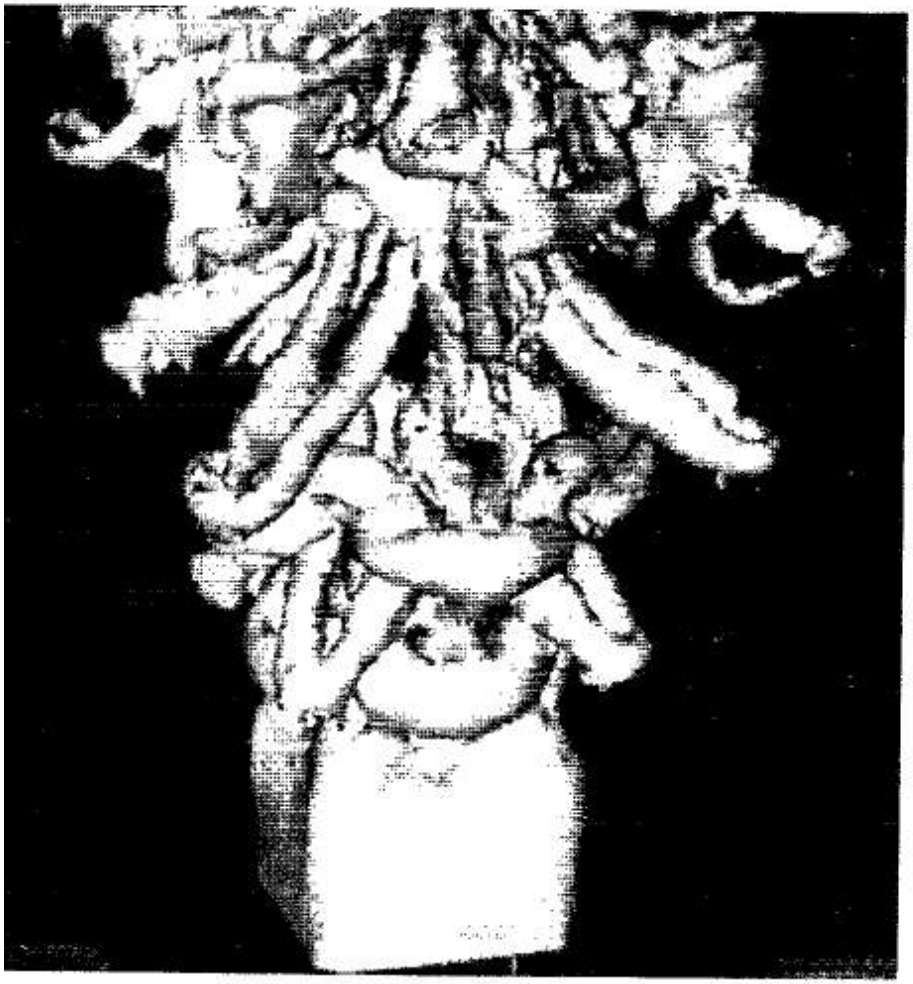

I, III, V : hairpin (braid) vortices
II, IV : deformed vortex rings

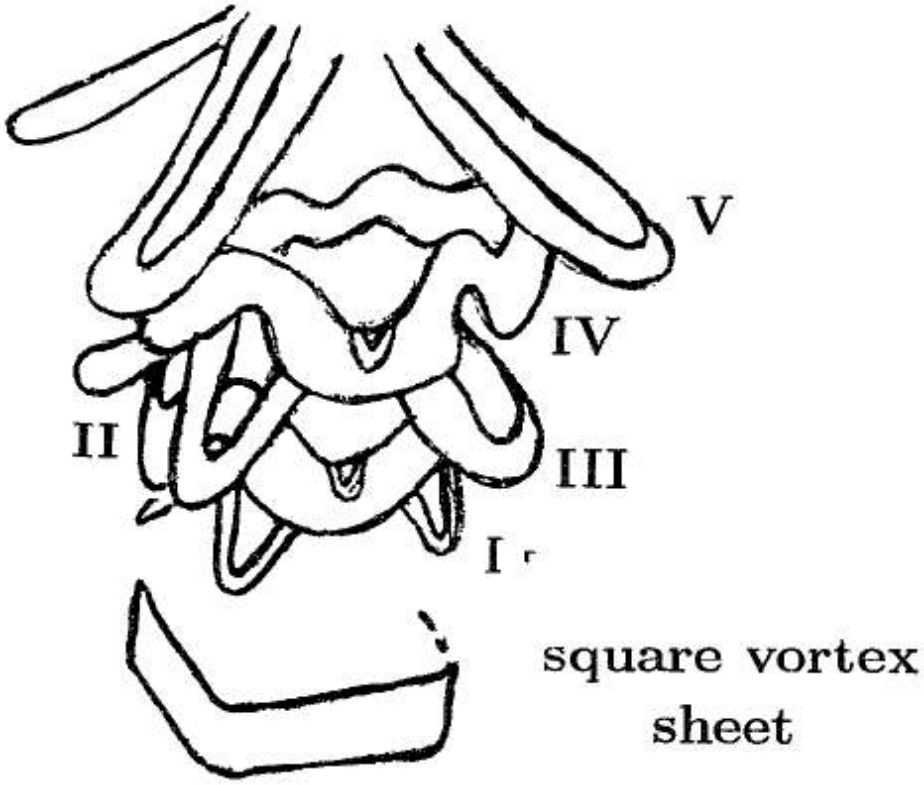

Annu. Rev. Fluid Mech. 1999. 31:239–72

FLOW| CONTROL WITH NONCIRCULAR JETS[1]

E. J. Gutmark
Mechanical Engineering Department, Louisiana State University, Baton Rouge, Louisiana 70803-6413; e-mail: gutmark@me.lsu.edu

F. F. Grinstein
Laboratory for Computational Physics and Fluid Dynamics, Code 6410, Naval Research Laboratory, Washington, DC 20375-5344; e-mail: grinstei@lcp.nrl.navy.mil

KEY WORDS: vortices, mixing, combustion, entrainment

FLOW CONTROL WITH NONCIRCULAR JETS[1]

E. J. Gutmark
Mechanical Engineering Department, Louisiana State University, Baton Rouge, Louisiana 70803-6413; e-mail: gutmark@me.lsu.edu

F. F. Grinstein
Laboratory for Computational Physics and Fluid Dynamics, Code 6410, Naval Research Laboratory, Washington, DC 20375-5344; e-mail: grinstei@lcp.nrl.navy.mil

KEY WORDS: vortices, mixing, combustion, entrainment

ABSTRACT

Noncircular jets have been the topic of extensive research in the last fifteen years. These jets were identified as an efficient technique of passive flow control that allows significant improvements of performance in various practical systems at a relatively low cost because noncircular jets rely solely on changes in the geometry of the nozzle. The applications of noncircular jets discussed in this review include improved large- and small-scale mixing in low- and high-speed flows, and enhanced combustor performance, by improving combustion efficiency, reducing combustion instabilities and undesired emissions. Additional applications include noise suppression, heat transfer, and thrust vector control (TVC).

The flow patterns associated with noncircular jets involve mechanisms of vortex evolution and interaction, flow instabilities, and fine-scale turbulence augmentation. Stability theory identified the effects of initial momentum thickness distribution, aspect ratio, and radius of curvature on the initial flow evolution. Experiments revealed complex vortex evolution and interaction related to self-induction and interaction between azimuthal and axial vortices, which lead to axis switching in the mean flow field. Numerical simulations described the details and clarified mechanisms of vorticity dynamics and effects of heat release and reaction on noncircular jet behavior.

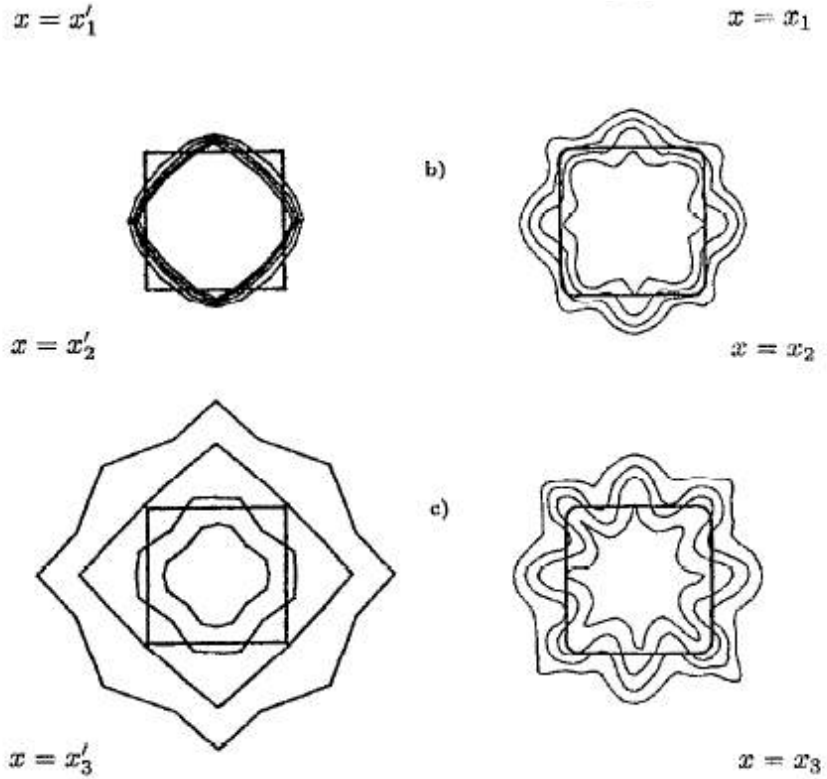

FIG. 10. Axis switching of the jet cross section in terms of isocontours of time-averaged streamwise velocity scaled with its local centerline value (u/u_{cl}) for experimental (OU1) and simulated (SQ1) jets. Contour levels are 0.2, 0.4, 0.6, and 0.8. The geometry of the experimental nozzle is superimposed on each slice on the left; the initial half-width velocity cross section of the simulated jets is superimposed on each slice on the right. The stream-

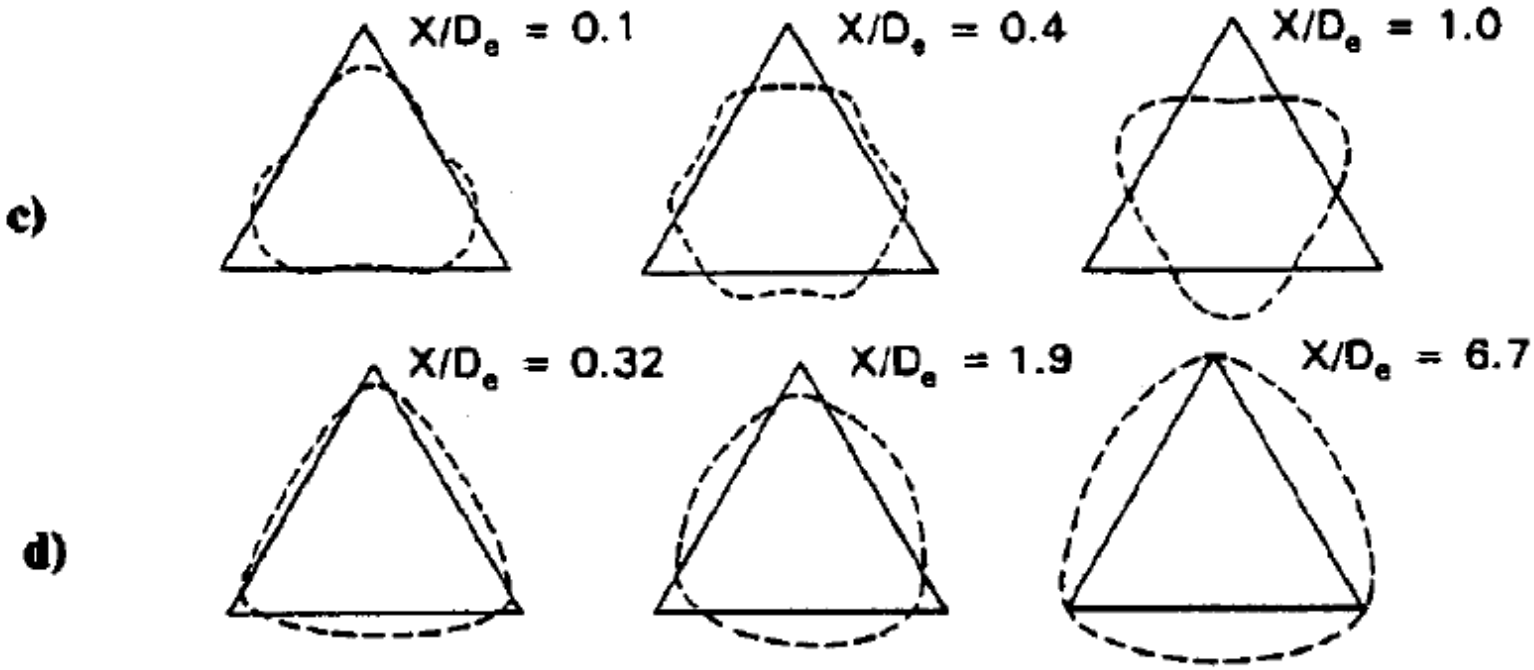

Figure 6 Variation of momentum thickness with axial distance at the vertex and flat sides of the triangular jet: (*a*) orifice jet, (*b*) pipe jet. Corresponding evolution of the jet cross-sections along the axis: (*c*) orifice jet, (*d*) pipe jet. (Koshigoe et al 1989)

Euler equations

u: velocity field

$\omega = \operatorname{curl} u = \nabla \wedge u$: vorticity

$\omega = \Gamma T ds \qquad T = X_s$

$X = X(s,t)$ curve in $\mathbb{R}^3$ support of ω

$\operatorname{div} u = 0$

$$u(P) = \frac{\Gamma}{4\pi} \int_{-\infty}^{\infty} \frac{X(s) - P}{|X(s) - P|^3} \wedge T(s) ds$$

Examples: straight lines, vortex rings, helical vortices

BINORMAL FLOW (Vortex Filament Flow)

$$X_t = X_s \wedge X_{ss} = cb$$

- $X = X(s,t) \in \mathbb{R}^3$
- $c = c(s,t)$ curvature
- $b = b(s,t)$ binormal

Examples:

a) circle

b) straight line

c) helix

Remark.–

- $X_s = T \qquad |T|^2 = \text{constant}$
- Time reversible equation : $\widetilde{X}(s,t) = X(-s,-t)$
- Rotation invariant

Non-linear equation(s)

$$X_t = X_s \wedge X_{ss} = cb$$

- $X = X(s,t) \in \mathbb{R}^3$
- $c = c(s,t)$ curvature
- $b = b(s,t)$ binormal

$$T_t = T \wedge T_{ss} = JD_sT_s \qquad |T| = 1$$

Hasimoto '70 $$\psi(s,t) = c(s,t)e^{i\int_0^s \tau(s',t)ds'}$$

$$\partial_t\psi(s,t) = i\left(\partial_s^2\psi \pm \frac{1}{2}(|\psi|^2 + A(t))\psi\right) \qquad A(t) \in \mathbb{R}$$

Conservation Laws (CLs)

- Cubic NLS is a completely integrable system.
  - No use of high order CLs.
  - Rough initial conditions.
- Kinetic energy $\int c^2 ds = \int |\psi|^2 ds = \int |T_s|^2 ds$.
- Total torsion $\int \tau ds$ (scaling invariant)
- Linear Momentum (Impulse): $\frac{1}{2}\int X \wedge T ds$.
- Angular Momentum: $\frac{1}{3}\int X \wedge (X \wedge T) ds$.

One corner

$$X(s,0) = \begin{cases} A_s^+ & s \geq 0 \\ A_s^- & s \leq 0. \end{cases}$$

$$T(s,0) = \begin{cases} A^+ & s > 0 \\ A^- & s < 0. \end{cases}$$

$$\psi(s,0) = a\delta$$

Q : **How does the corner move?**

$$X_t = cb$$

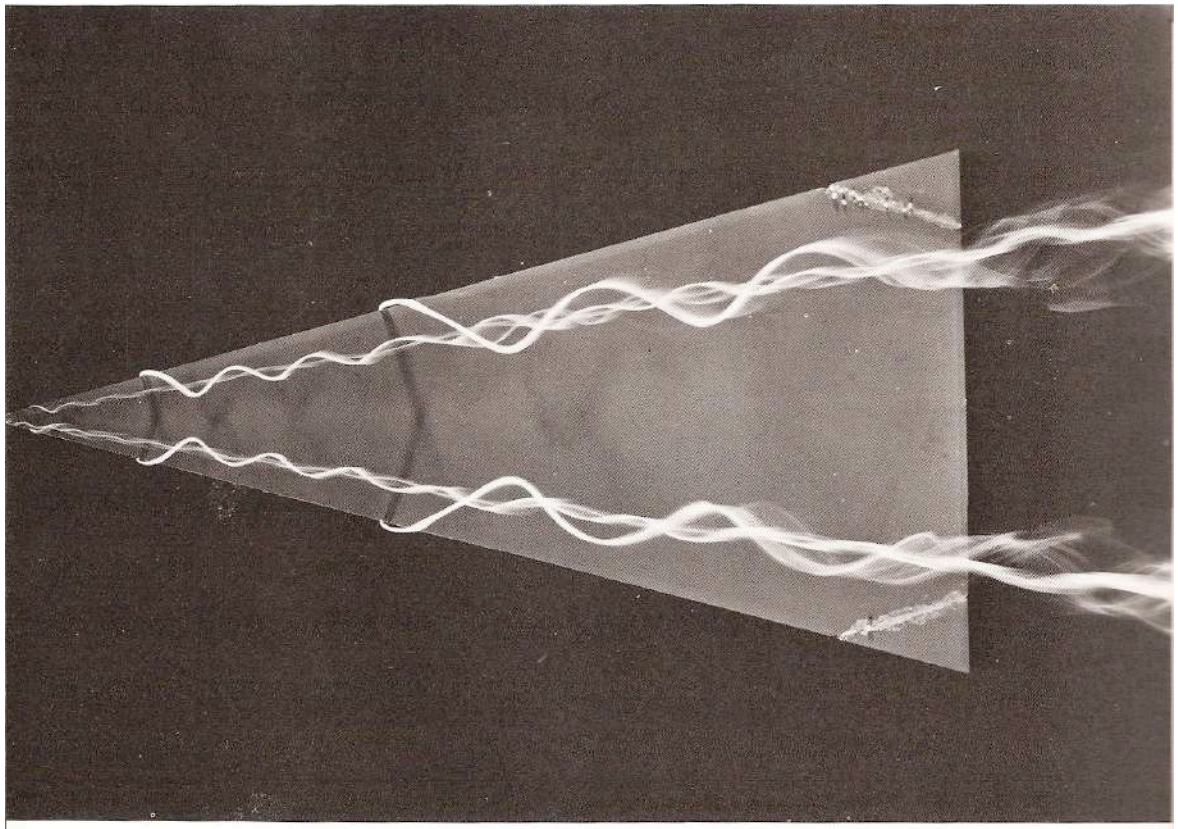

90. Vortices above an inclined triangular wing. Lines of colored fluid in water show the symmetrical pair of vortices behind a thin wing of 15° semi-vertex angle at 20° angle of attack. The Reynolds number is 20,000 based on chord. Although the Mach number is very low, the flow field is practically conical over most of the wing, quantities being constant along rays from the apex. ONERA photograph, *Werlé 1963*

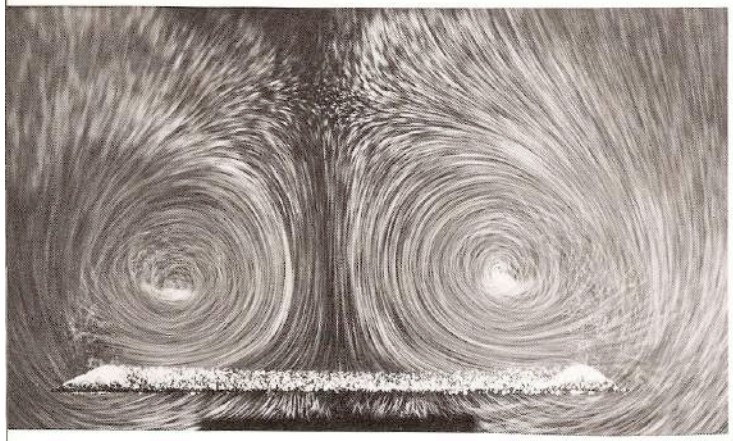

91. Cross section of vortices on a triangular wing. Tiny air bubbles in water show the vortex pair for the flow above in a section at the trailing edge of the wing. ONERA photograph, *Werlé 1963*

One corner

$$X(s,t) = \sqrt{t}G\left(s/\sqrt{t}\right) \qquad T(s,t) = T\left(s/\sqrt{t}\right)$$

$$T_t = T \wedge T_{ss}$$

Differentiating and making $t = 1$

$$\frac{1}{2}G - \frac{s}{2}G' = G' \wedge G'' \ (= cb)$$

Frenet equations:

$$\begin{aligned} T' &= cn \\ n' &= -cT + \tau b \\ b' &= -\tau n \end{aligned}$$

$$\begin{aligned} -\frac{s}{2}cn &= T \wedge \left(c'n - c^2T + c\tau b\right) \\ c' &= 0 \qquad c = a \qquad \tau = s/2 \end{aligned}$$

Buttke'88

$$\mathbf{G(0) = 2ab(0)}$$

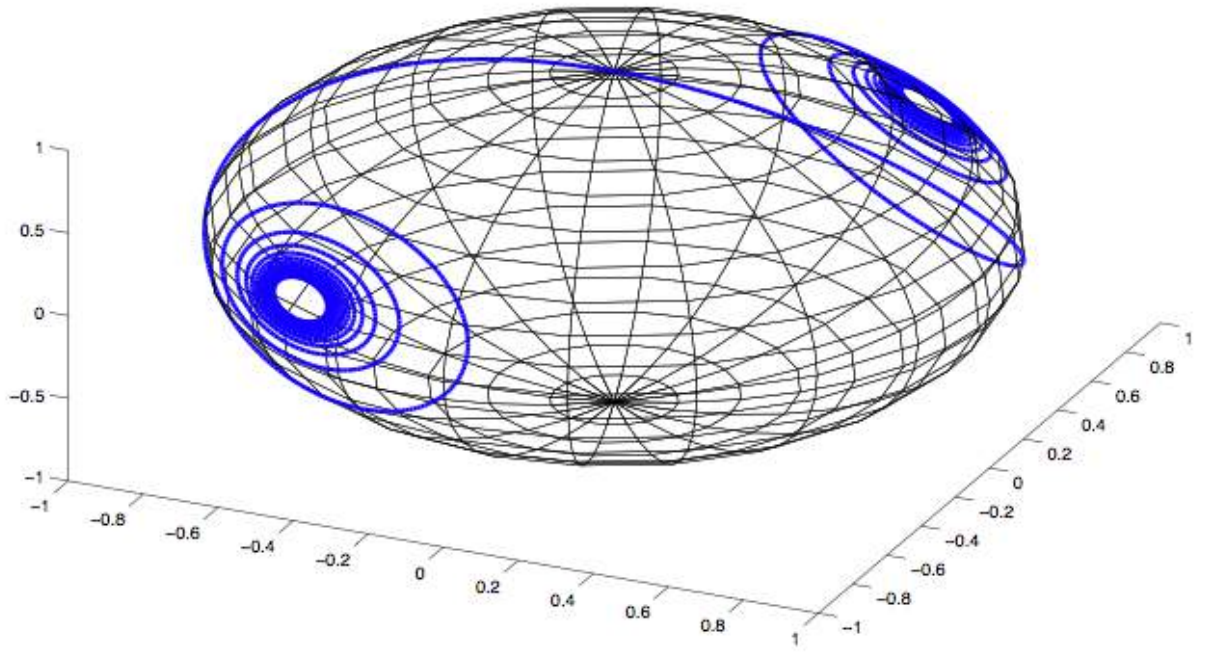
1
0.5
0
−0.5
−1
−1
−0.8
−0.6
−0.4
−0.2
0
0.2
0.4
0.6
0.8
1
−1
−0.8
−0.6
−0.4
−0.2
0
0.2
0.4
0.6
0.8
1

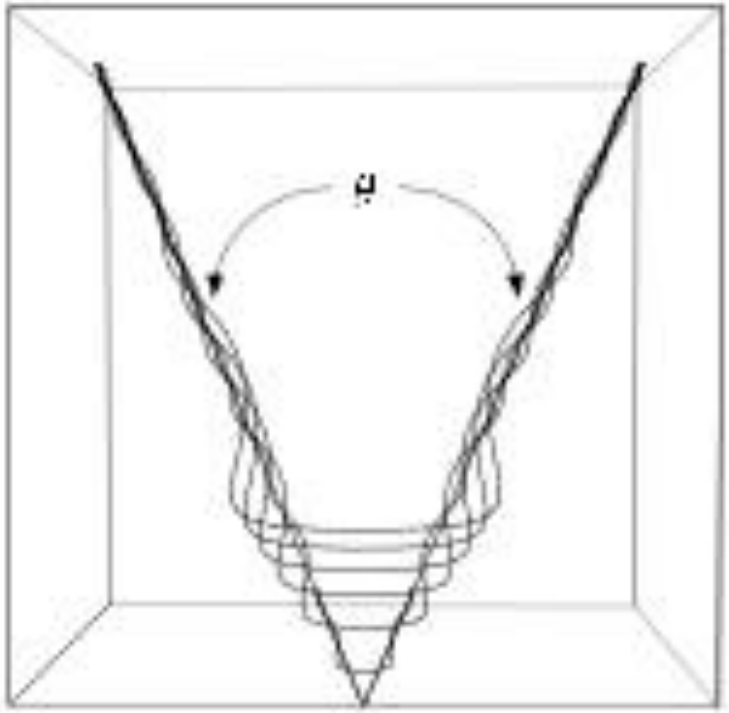

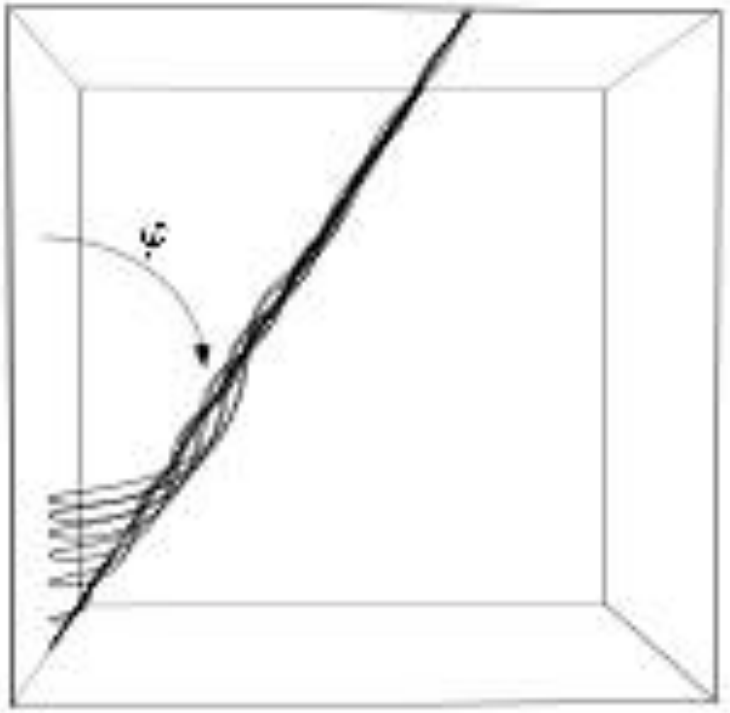

Theorem.– (Gutierrez, Rivas, V., '03) Given any two unit vectors (A^-, A^+), $A^\pm = (A_1^\pm, A_2^\pm, A_3^\pm)$ such that $A_3^\pm = 0$, there exists a unique G^a such that if

$$X(s,t) = \sqrt{t}\, G^a(s/\sqrt{t}) \quad \text{for } t > 0$$

then

$$X_t = X_s \wedge X_{ss} \quad ; \quad X(s,0) = \begin{cases} A^+ s & s \geq 0 \\ A^- s & s \leq 0. \end{cases}$$

Moreover, for $s \to \pm\infty$ there exist unit vectors (B^-, B^+) s.t.

(i) $G^a(s) = A^\pm\Big(s + 2\frac{a^2}{s}\Big) - 4\frac{a}{s^2} n_a + \mathcal{O}\Big(\frac{1}{|s|^2}\Big)$,

$T^a(s) = A^\pm - \frac{2a}{s} b^a + \mathcal{O}\Big(\frac{1}{|s|}\Big)$,

$(n^a - ib^a)(s) = B^\pm e^{i\frac{s^2}{4} + ia^2 \lg|s|} + O\Big(\frac{1}{|s|}\Big)$.

(ii) $\sin\frac{\widehat{(A^+, -A^-)}}{2} = e^{-\pi\frac{a^2}{2}}$; $\sin\varphi = \frac{A_2}{\sqrt{1-A_1^2}}$.

(iii) $\widehat{G_3^a} \neq 0 \qquad \lim_{|\xi|\to\infty} |\xi|\,|\widehat{T_3^a}| = \eta_a > 0.$

Corollary.– As before,

$$T(s,t) = T^a(s/\sqrt{t}) \quad ; \quad T(s,0) = \begin{cases} A^+ & s > 0 \\ A^- & s < 0. \end{cases}$$

Then, for $t > 0$,

(i) $$\|T(\cdot,t)\|^2_{B^{1/2}_{2,\infty}} = \|T^a\|^2_{B^{1/2}_{2,\infty}}$$
$$\geq \|T(\cdot,0)\|^2_{B^{1/2}_{2,\infty}} + \eta_a^2 > \|T(\cdot,0)\|^2_{B^{1/2}_{2,\infty}}$$

(ii) $$\int X \wedge T ds = t \int G^a \wedge T^a ds = t(A^+ - A^-) = 2te^{-\pi \frac{a^2}{2}}.$$

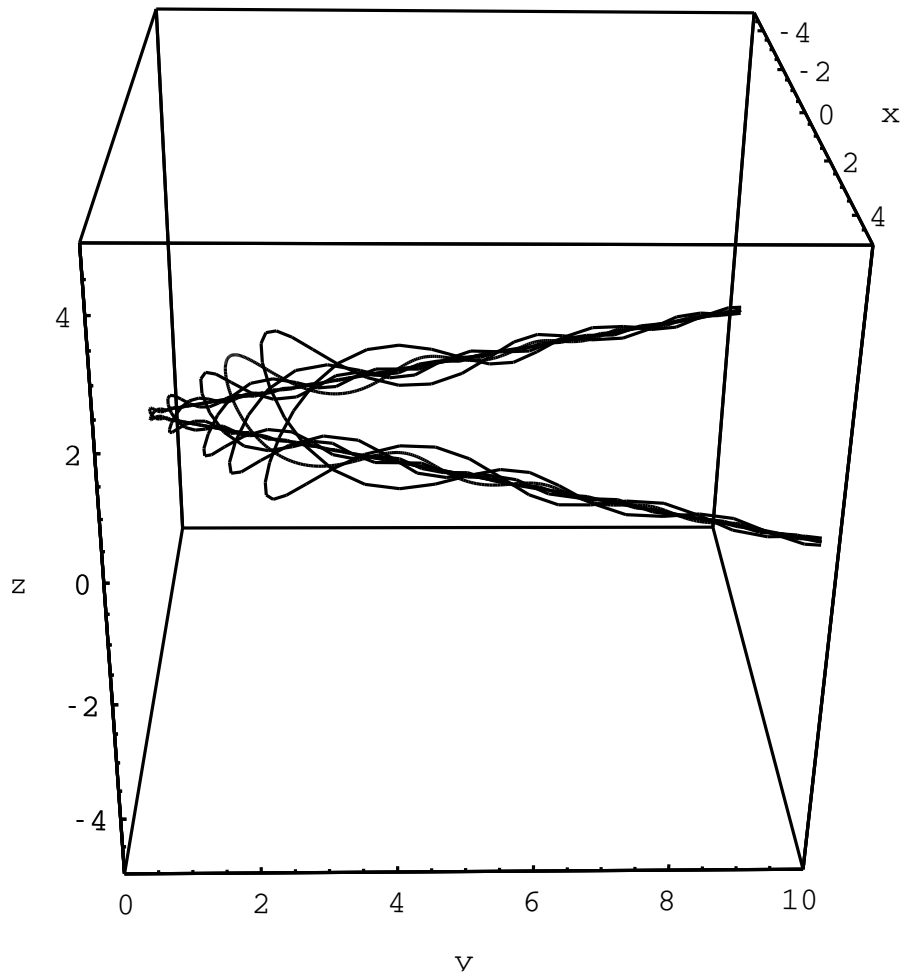

Theorem.– (with V. Banica) The self-similar solutions are stable. In particular, the creation/annilihation of a corner is stable.

V. Banica 2008-2014

- Conformal transformation of ψ: existence of wave operator and asymptotic completeness.

- The right space of functions.

- Long range potential: Cubic NLS with the Dirac–delta as initial condition is ill–posed.

- The recipe to go beyond $t = 0$: Blow–up argument to "capture" the selfsimilar solution

- The characterization of the selfsimilar solutions plays a fundamental role.

S. Gutiérrez, J. Rivas 2003

A REGULAR POLYGON (with F. de la Hoz)

$$\psi(s,0) = \frac{2\pi}{M} \sum_{k=-\infty}^{\infty} \delta\left(s - \frac{2\pi k}{M}\right).$$

- Galilean Transformations

$$\tilde{\psi}(s,t) \equiv e^{iks - ik^2 t}\psi(s - 2kt, t), \quad \forall\, k, t \in \mathbb{R}.$$

$$e^{2\pi i j M s}\psi(s,0) = \psi(s,0) \quad \forall\, j \in \mathbb{Z}.$$

$$\tilde{\psi}_k = \psi \quad \forall\, k \in \mathbb{Z}.$$

$$
\begin{aligned}
\psi\left(s,t_{pq}\right) &= \widehat{\psi}\left(0,t_{pq}\right)\sum_{k=-\infty}^{\infty}e^{-i(Mk)^{2}2\pi p/(M^{2}q)+iMks} \\
&= \widehat{\psi}\left(0,t_{pq}\right)\sum_{k=-\infty}^{\infty}e^{-2\pi i(p/q)k^{2}+iMks} \\
&= \widehat{\psi}\left(0,t_{pq}\right)\sum_{l=0}^{q-1}\sum_{k=-\infty}^{\infty}e^{-2\pi i(p/q)(qk+l)^{2}+iM(qk+l)s} \\
&= \widehat{\psi}\left(0,t_{pq}\right)\sum_{l=0}^{q-1}e^{-2\pi i(p/q)l^{2}+iMls}\sum_{k=-\infty}^{\infty}e^{iMqks}.
\end{aligned}
$$

The generalized quadratic Gauß sums are defined by

$$\sum_{l=0}^{|c|-1} e^{2\pi i(al^2+bl)/c},$$

for given integers a, b, c, with $c \neq 0$.

$$G(-p,m,q) = \begin{cases} \sqrt{q}e^{i\theta_m}, & \text{if } q \text{ is odd,} \\ \sqrt{2q}e^{i\theta_m}, & \text{if } q \text{ is even and } q/2 \equiv m \mod 2, \\ 0, & \text{if } q \text{ is even and } q/2 \not\equiv m \mod 2, \end{cases}$$

for a certain angle θ_m that depends on m (and, of course, on p and q, too).

$$\begin{pmatrix} \mathrm{T} \\ \mathrm{e}_1 \\ \mathrm{e}_2 \end{pmatrix}_s = \begin{pmatrix} 0 & \alpha & \beta \\ -\alpha & 0 & 0 \\ -\beta & 0 & 0 \end{pmatrix} \cdot \begin{pmatrix} \mathrm{T} \\ \mathrm{e}_1 \\ \mathrm{e}_2 \end{pmatrix} .$$

$$\begin{pmatrix} \mathrm{T} \\ \mathrm{e}_1 \\ \mathrm{e}_2 \end{pmatrix}_s = \begin{pmatrix} 0 & a\delta & b\delta \\ -a\delta & 0 & 0 \\ -b\delta & 0 & 0 \end{pmatrix} \cdot \begin{pmatrix} \mathrm{T} \\ \mathrm{e}_1 \\ \mathrm{e}_2 \end{pmatrix} .$$

$$\begin{pmatrix} u_1(0^+) \\ u_2(0^+) \\ u_3(0^+) \end{pmatrix} = \exp\left[\begin{pmatrix} 0 & a & b \\ -a & 0 & 0 \\ -b & 0 & 0 \end{pmatrix} \int_{0^-}^{0^+} \delta(s')ds'\right] \cdot \begin{pmatrix} u_1(0^-) \\ u_2(0^-) \\ u_3(0^-) \end{pmatrix}$$

$$= \exp\left[\begin{pmatrix} 0 & a & b \\ -a & 0 & 0 \\ -b & 0 & 0 \end{pmatrix}\right] \cdot \begin{pmatrix} u_1(0^-) \\ u_2(0^-) \\ u_3(0^-) \end{pmatrix}$$

$$\left(\begin{array}{c} \mathrm{T}\left(\frac{2\pi k}{Mq}^{+}\right)^{T} \\ \hline \mathrm{e}_1\left(\frac{2\pi k}{Mq}^{+}\right)^{T} \\ \hline \mathrm{e}_2\left(\frac{2\pi k}{Mq}^{+}\right)^{T} \end{array}\right) = \mathrm{M}_k \cdot \mathrm{M}_{k-1} \cdot \ldots \cdot \mathrm{M}_1 \cdot \mathrm{M}_0 \cdot \left(\begin{array}{c} \mathrm{T}\,(0^{-})^{T} \\ \hline \mathrm{e}_1\,(0^{-})^{T} \\ \hline \mathrm{e}_2\,(0^{-})^{T} \end{array}\right)$$

$$\mathrm{M}_{Mq-1} \cdot \mathrm{M}_{Mq-2} \cdot \ldots \cdot \mathrm{M}_1 \cdot \mathrm{M}_0 \equiv \mathrm{I}.$$

Let us define

$$\mathrm{M} = \mathrm{M}_{q-1} \cdot \mathrm{M}_{q-2} \cdot \ldots \cdot \mathrm{M}_1 \cdot \mathrm{M}_0.$$

- M is an M–th root of the identity matrix.
- M is a rotation matrix that induces a rotation of $2\pi/M$ degrees around a certain rotation axis.

$$\mathrm{Tr}\,(\mathrm{M}) = 1 + 2\cos\left(\frac{2\pi}{M}\right),$$

$$\sigma(\mathrm{M}) = \left\{1, e^{2\pi i/M}, e^{-2\pi i/M}\right\}.$$

$$\cos(\rho) = \begin{cases} 2\cos^{2/q}(\pi/M) - 1, & \text{if } q \text{ is odd}, \\ 2\cos^{4/q}(\pi/M) - 1, & \text{if } q \text{ is even}, \end{cases}$$

The generalized quadratic Gauß sums are defined by

$$\sum_{l=0}^{|c|-1} e^{2\pi i(al^2+bl)/c},$$

for given integers a, b, c, with $c \neq 0$.

$$G(-p,m,q) = \begin{cases} \sqrt{q}e^{i\theta_m}, & \text{if } q \text{ is odd,} \\ \sqrt{2q}e^{i\theta_m}, & \text{if } q \text{ is even and } q/2 \equiv m \mod 2, \\ 0, & \text{if } q \text{ is even and } q/2 \not\equiv m \mod 2, \end{cases}$$

with

$$\theta_m \text{“} = \text{”} \, 2\pi i \tfrac{\phi(p)}{q}(2m+1)$$

$$\phi(p) = (4p)^{-1} \mod q$$

(Explicit inversive congruential generators, Eichenaber-Herrmann, ’93

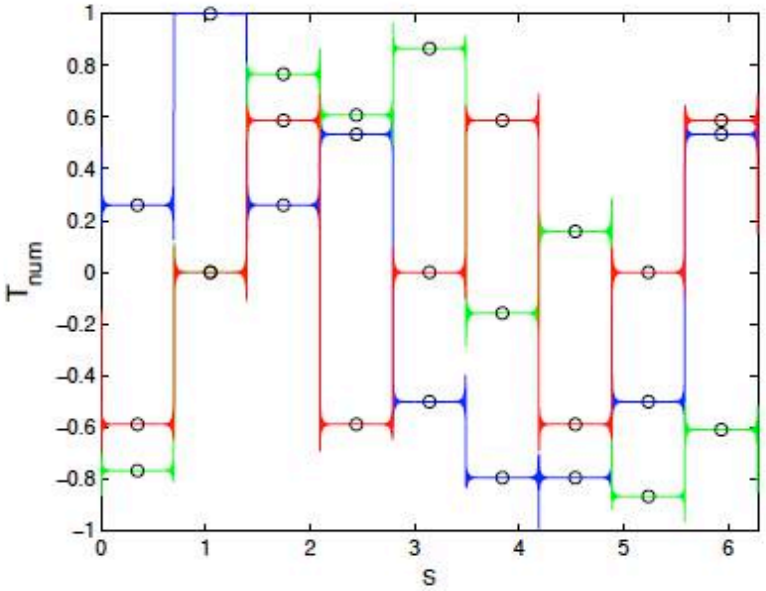

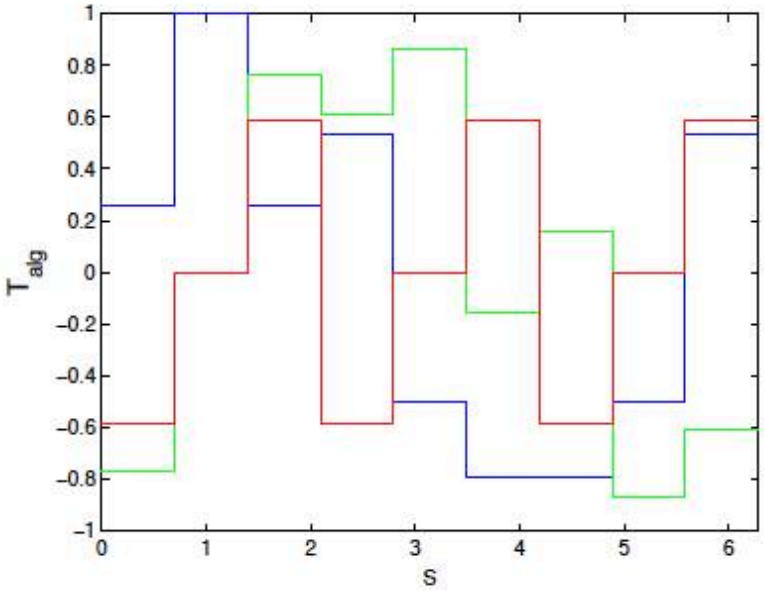

$\mathbf{T}_{num}$ versus $\mathbf{T}_{alg}$, for $M = 3$, at $T_{1,3} = \dfrac{2\pi}{27}$. T_1 appears in blue, T_2 in green, T_3 in red. In $\mathbf{T}_{num}$, the Gibbs phenomenon is clearly visible. The black circles denote the points chosen for the comparisons.

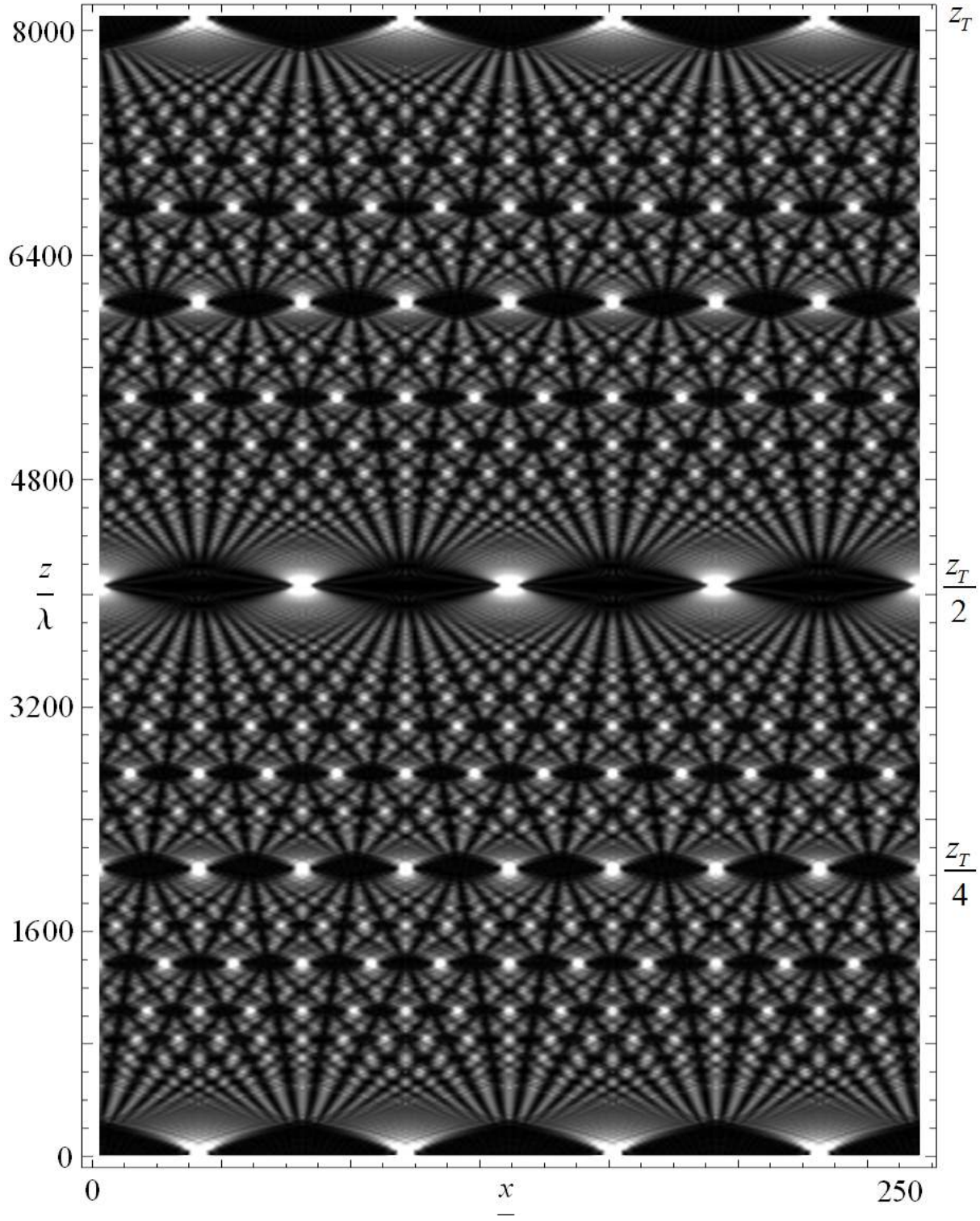
8000
6400
4800
$\frac{z}{\lambda}$
3200
1600
0
0
$\frac{x}{\lambda}$
250
z_T
$\frac{z_T}{2}$
$\frac{z_T}{4}$

$$\phi(t) = \int_0^t \left(\sum_{k=1}^{\infty} e^{\pi i k^2 \tau} \right) d\tau = a_0 + \sum_{k \neq 0} \frac{e^{\pi i k^2 t}}{i \pi k^2}, \quad t \in [0, 2]$$

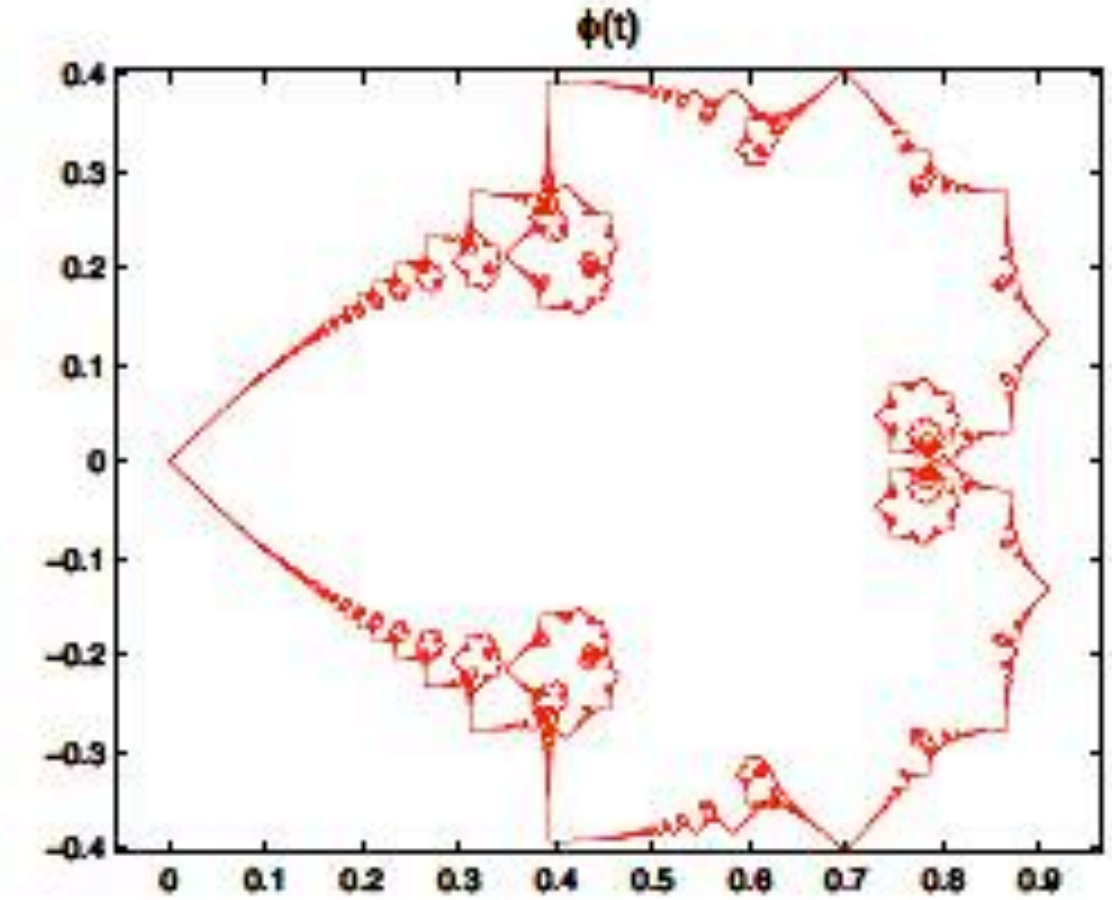

- Jaffard
- Multifractal (Frisch–Parisi conjecture)

- Berry and Goldberg, Talbot Effect ’88,
- Duistermaat ’91,
- Oskolkov ’92,
- Jaffard, multifractal ’96,
- Kapitanski, Rodnianski ’99,
- Olver ’10,
- Erdogan, Tzirakis ’13,
- Chousionis, Erdogan, Tzirakis ’15.

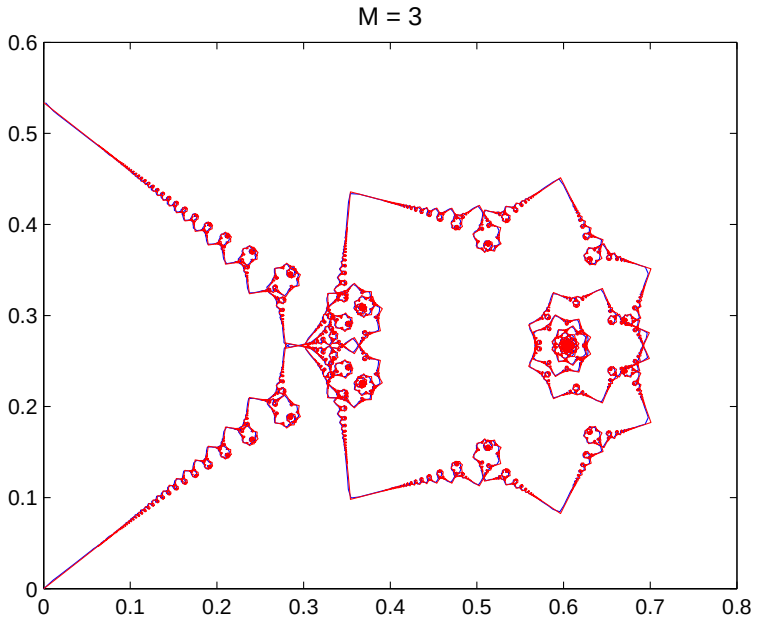
M = 3
0.6
0.5
0.4
0.3
0.2
0.1
0
0
0.1
0.2
0.3
0.4
0.5
0.6
0.7
0.8

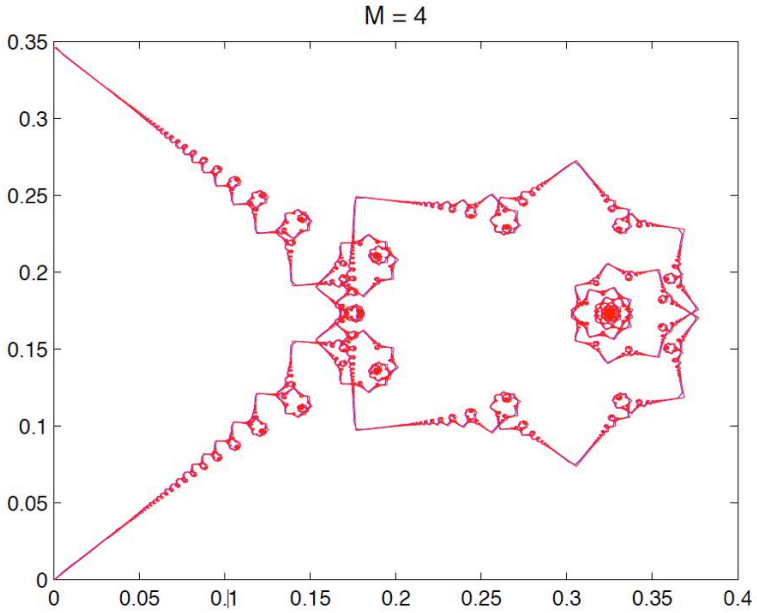
M = 4
0.35
0.3
0.25
0.2
0.15
0.1
0.05
0
0
0.05
0.1
0.15
0.2
0.25
0.3
0.35
0.4

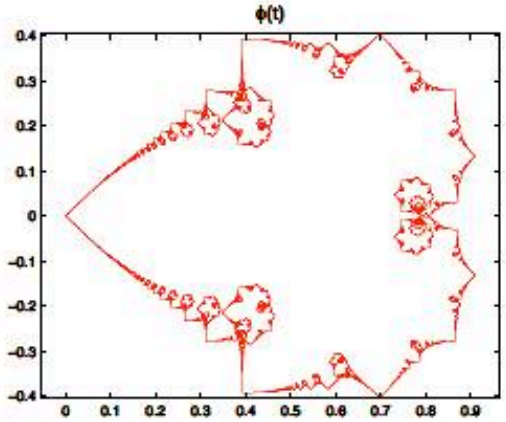
φ(t)

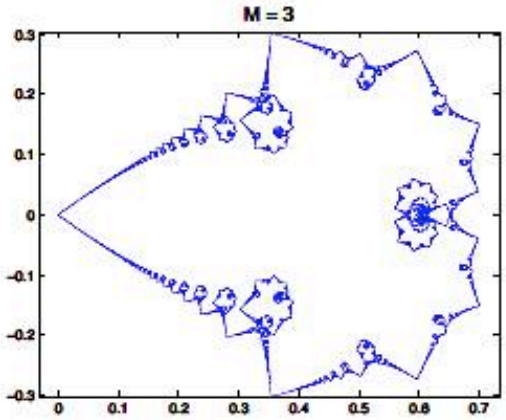
M = 3

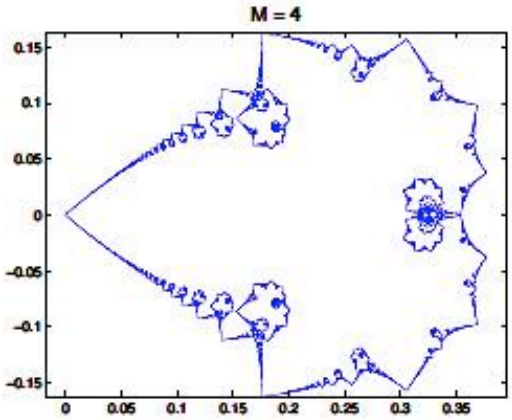
M = 4

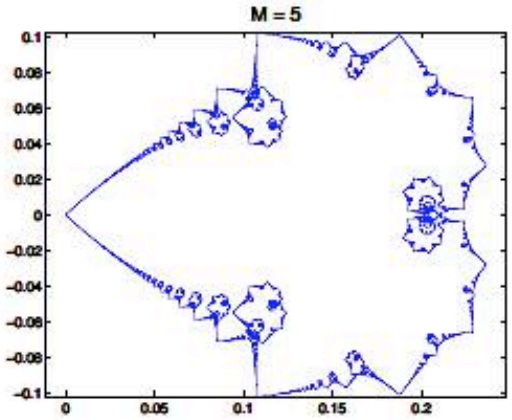
M = 5

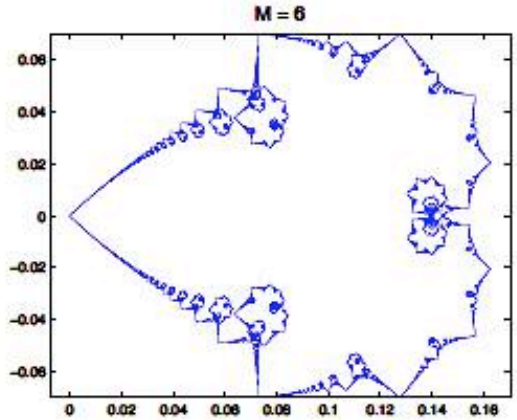
M = 6

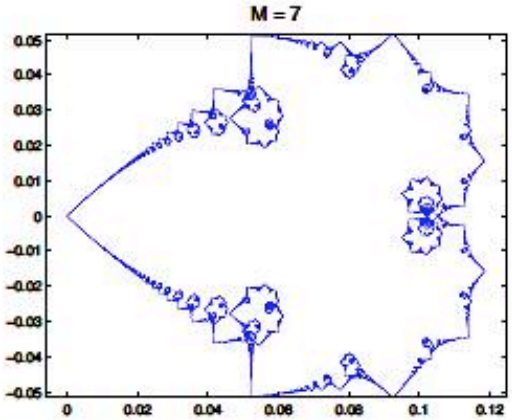
M = 7

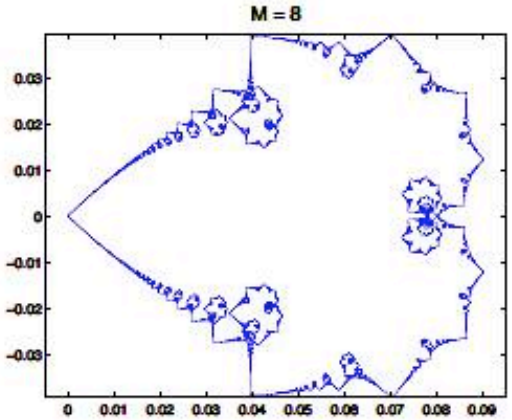
M = 8

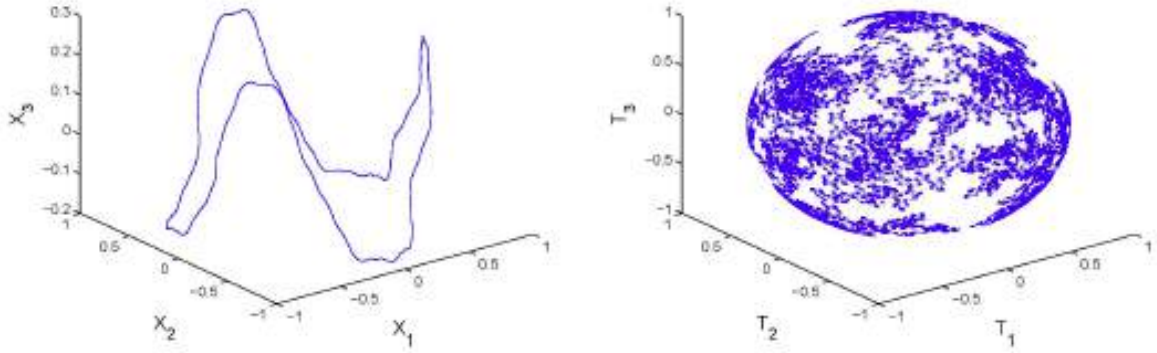

Figure 8: $\mathbf{X}_{alg}$ and $\mathbf{T}_{alg}$, at $t = \frac{2\pi}{9}(\frac{1}{4} + \frac{1}{41} + \frac{1}{401}) = \frac{2\pi}{9} \cdot \frac{18209}{65764}$.

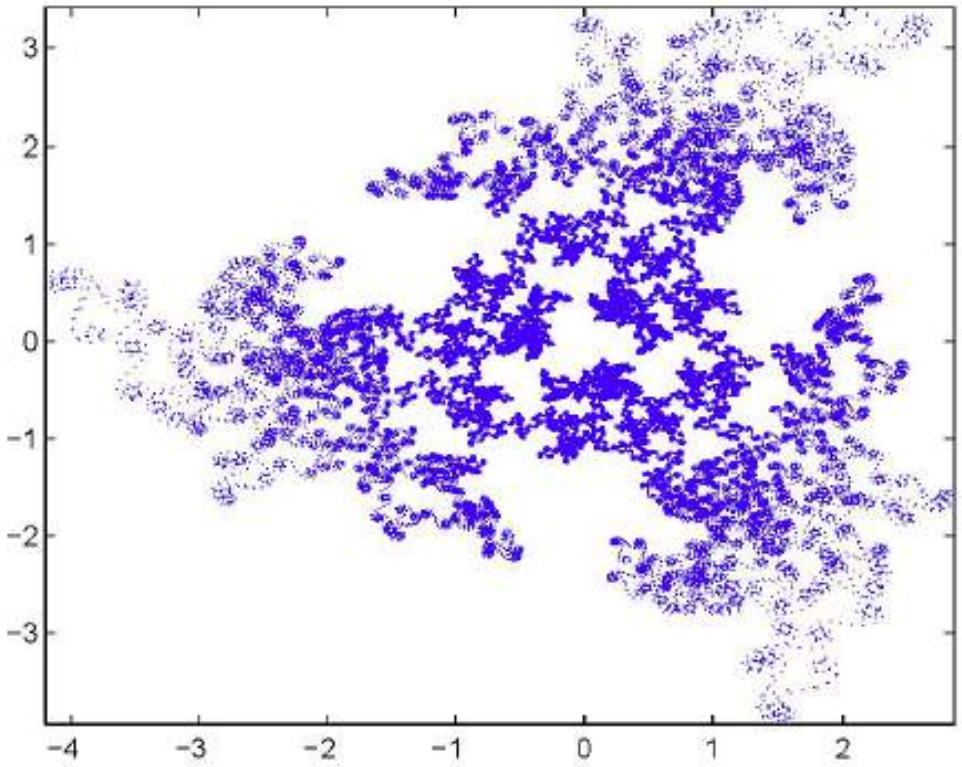

Figure 9: Stereographic projection of the right-hand side of Figure 8.

THANK YOU FOR YOUR ATTENTION

Pseudo-random numbers

Theorem.– Let us consider the triple product of three consecutive tangent vectors, and the scalar product of a tangent vector and the second next one. Then, these quantities depend exclusively on $\phi(p)$:

$$\phi(p) \equiv \begin{cases} (4p)^{-1} \bmod q, & \text{if } q \equiv 1 \bmod 2, \\ p^{-1} \bmod (q/2), & \text{if } q \equiv 2 \bmod 4, \\ p^{-1} \bmod q, & \text{if } q \equiv 0 \bmod 4. \end{cases}$$

Furthermore, taking the first quantity as the real part and the second quantity as the imaginary part of a complex number $z_{q,m}(p)$ that lies on a circumference of center $i\cos^2(\rho)$ and radius $\sin^2(\rho)$, for all p:

$$z_{q,m}(p) = \begin{cases} i\,c_\rho^2 - i\,s_\rho^2 \exp\left(\frac{2\pi i \phi(p)(2m+1)}{q}\right), & \text{if } q \not\equiv 2 \bmod 4, \\ i\,c_\rho^2 - i\,s_\rho^2 \exp\left(\frac{2\pi i \phi(p) m}{q/2}\right), & \text{if } q \equiv 2 \bmod 4. \end{cases}$$

Inversive congruential generators (ICGs), (Eichenauer 1986)

$$x_{n+1} \equiv \begin{cases} a\,\overline{x}_n + b \bmod q, & x_n \geq 1, \\ b, & x_n = 0, \end{cases} \qquad \overline{x} = x^{-1} \qquad n \geq 0,$$

with q prime, $a \not\equiv 0 \bmod q$:

- Absence of any lattice structure,
- Computational generation is not so efficient as with the Linear Congruential Generators.

Explicit inversive congruential generators (EICGs), (1993 Eichenauer–Herrmann):

$$x_n \equiv \overline{an + b} \bmod q, \quad n \geq 0,$$

with q prime, $a \not\equiv 0 \bmod q$; (full period i.e., $\{x_0, \ldots, x_{q-1}\} = \mathbb{Z}_q$).

- $u_n = x_n/q$ passes the uniformity test for equidistribution in $[0, 1)$.
- Behave very well in parallel and vector computations, as shown by Niederreiter: "*eminently suitable for the generation of parallel streams of pseudorandom numbers with desirable properties*".

- statistical independence properties; the discrepancy:

  for a given dimension $k \geq 2$ and for N arbitrary points $(\xi_0, \ldots, \xi_{N-1}) \in [0,1)^k$, to consider their discrepancy, which is defined as

$$D_N(\xi_0, \ldots, \xi_{N-1}) = \sup_J |F_N(J) - V(J)|,$$

  where the supremum is extended over all the subintervals J of $[0,1)^k$; $F_N(J)$ is N^{-1} times the number of terms among $\xi_0, \ldots, \xi_{N-1}$ falling into J; and $V(J)$ denotes the volume of J.

Eeichenauer(1993): given a sequence of numbers $(u_n)_{n\geq 0}$ obtained with an EICG, the k-dimensional points

$$\mathbf{u}_n = (u_{n+n_1}, \ldots, u_{n+n_k}) \in [0,1)^k, \quad 0 \leq n < p,$$

is considered, for $n_1, \ldots, n_k$ arbitrary integers satisfying $0 = n_1 < \ldots < n_k < p$, and the abbreviation

$$D_p^{(k)} = D_p(\mathbf{u}_0, \ldots, \mathbf{u}_{p-1})$$

being used for their discrepancy.

- For EICG, $p^{-1/2} < D_p^{(k)} < p^{-1/2}(\log p)^k$.

  Versus $p^{-1/2}(\log\log p)^{1/2}$ for p independent and uniformly distributed points taken from $[0,1)^k$.

- Behave very well in parallel and vector computations, as shown by Niederreiter: "*eminently suitable for the generation of parallel streams of pseudorandom numbers with desirable properties*".

- **The Talbot effect. The linear setting.**

- **The Talbot efffect. The non–linear setting.**
  V. Banica, F. de la Hoz.

- **Pictures.**

Q: Has the Talbot effect anything to do with turbulence?


Pergamon

0045-7930(94)00019-0

Computers & Fluids Vol. 24, No. 1, pp. 1–25, 1995

0045-7930/95 $9.50 + 0.00

NUMERICAL SIMULATION OF NON-CIRCULAR JETS

R. S. MILLER, C. K. MADNIA and P. GIVI†
Department of Mechanical and Aerospace Engineering, State University of New York at Buffalo, Buffalo, NY 14260-4400, U.S.A.

(Received 3 January 1994; in revised form 16 May 1994)

Abstract—Results are presented of numerical simulations of spatially developing, three-dimensional jets issued from circular and non-circular nozzles of identical equivalent diameters. Elliptic, rectangular and triangular jets are considered with aspect-ratios of 1:1 and 2:1. Flow visualization results show that large scale coherent structures are formed in both cornered and non-cornered jets. The axis-switching phenomenon is captured in all non-unity aspect-ratio jets and also in the equilateral triangular jet. The

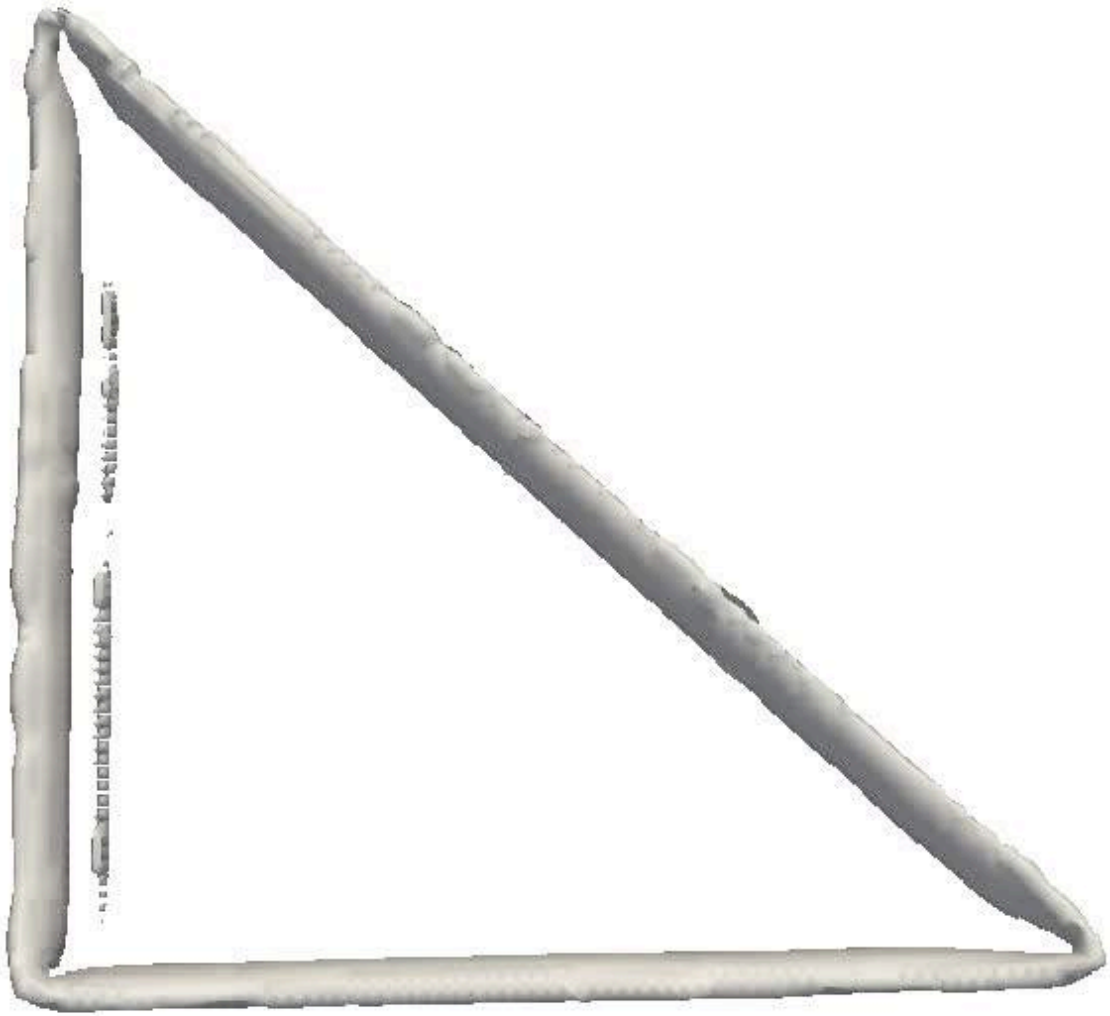

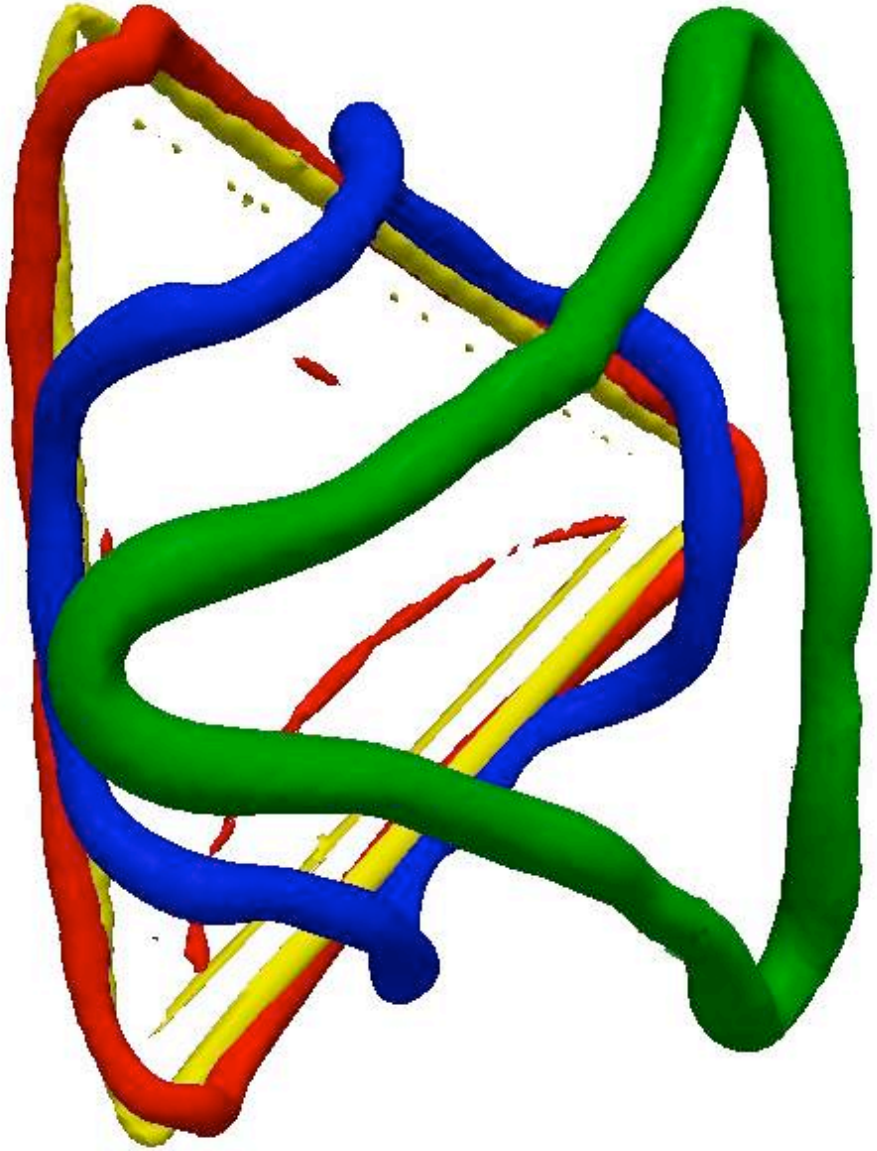

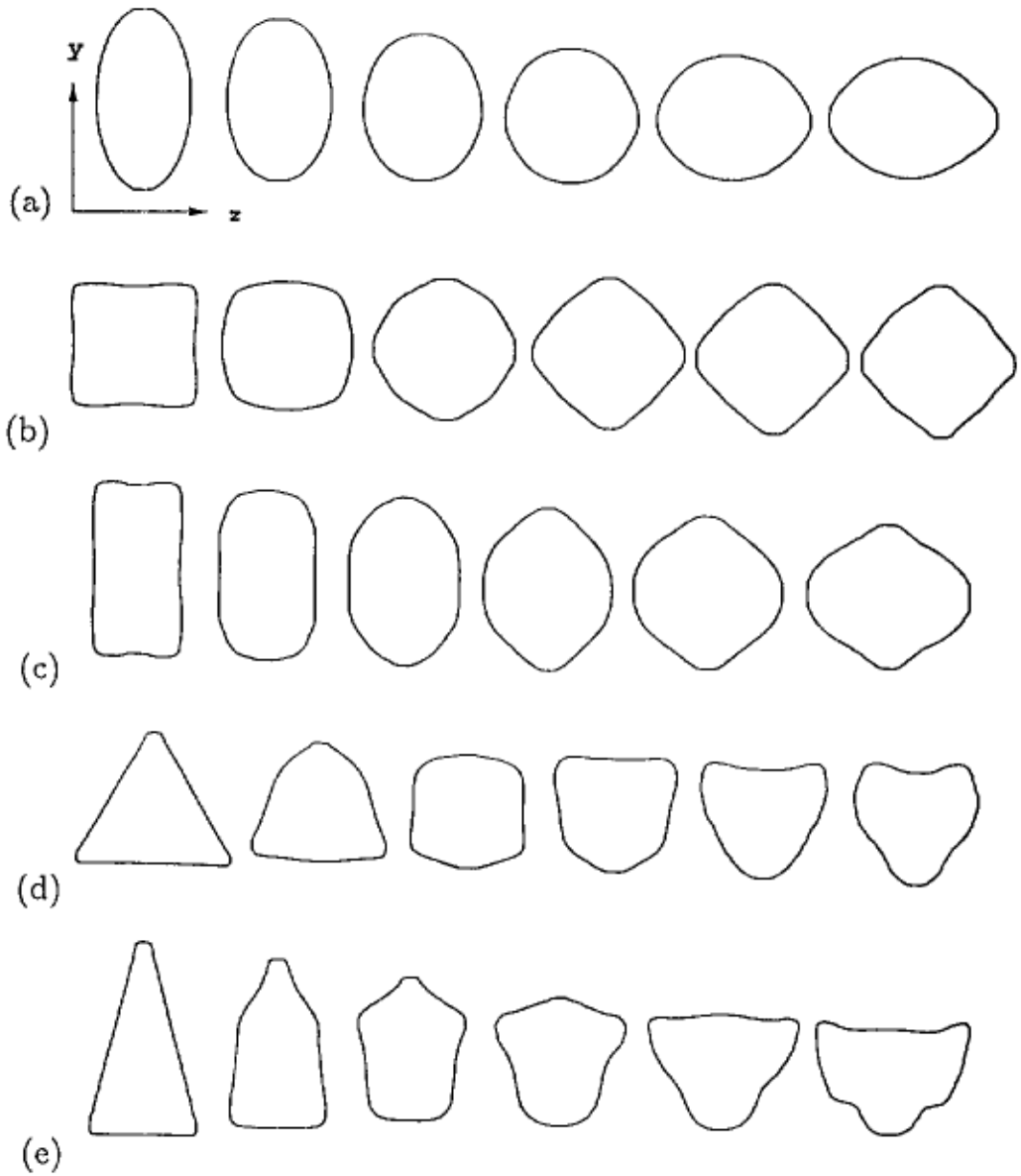

Fig. 8. Axis switching as depicted by $\langle U_h \rangle$ contours. Contours are in increments of $x^* = 1$. (a) Run 2, (b) Run 3, (c) Run 4, (d) Run 5, (e) Run 6.

Theorem 2.1. *([9]) Given $a > 0$ then the family of curves*

$$\chi_a(t,x) = \sqrt{t}\, G_a\left(\frac{x}{\sqrt{t}}\right),$$

with G_a given in (23) (i.e. the Frenet frame (T_a, n_a, b_a) at $x = 0$ is the canon thonormal basis of $\mathbb{R}^3$) is a solution of the binormal flow which is real analytic fo Moreover, there exist $A_a^{\pm}$ and $B_a^{\pm}$ such that

(i)

$$|\chi_a(t,x) - A^+ x\, \mathbf{1}_{[0,\infty[}(x) - A^- x\, \mathbf{1}_{]-\infty,0]}(x)| \leq a\sqrt{t},$$

(ii) The following asymptotics hold, for $s \to \pm\infty$:

$$G_a(s) = A_a^{\pm}\left(s + \frac{2a^2}{s}\right) - \frac{4a}{s^2}\, n_a + \mathcal{O}\left(\frac{1}{s^3}\right),$$

$$T_a(s) = A_a^{\pm} - \frac{2a}{s}\, b_a + \mathcal{O}\left(\frac{1}{s^2}\right),$$

$$(n_a - i b_a)(s) = B_a^{\pm}\, e^{i\frac{s^2}{4t}}\, e^{ia^2 \log|s|} + \mathcal{O}\left(\frac{1}{s}\right),$$

(iii) The real vectors $A_a^{\pm} = (A_{a,1}^{\pm}, A_{a,2}^{\pm}, A_{a,3}^{\pm})$ are unitary and

$$A_{a,1}^+ = A_{a,1}^- = e^{-\pi\frac{a^2}{2}}, \quad A_{a,2}^+ = -A_{a,2}^-, \quad A_{a,3}^+ = -A_{a,3}^-, \quad A_a^{\pm} \perp B_a^{\pm},$$

(iv) The complex vectors $B_a^{\pm} = (B_{a,1}^{\pm}, B_{a,2}^{\pm}, B_{a,3}^{\pm})$ verify $|\Re B_a^{\pm}| = |\Im B_a^{\pm}| = 1$ and

$$B_{a,1}^+ = -B_{a,1}^-, \quad B_{a,2}^+ = B_{a,2}^-, \quad B_{a,3}^+ = B_{a,3}^-, \tag{25}$$

(v) The angle of the corner of $\chi_a(0)$ is determined by

$$\sin\frac{\widehat{(A^+, -A^-)}}{2} = A_{a,1}^{\pm} = e^{-\pi\frac{a^2}{2}}.$$